NRC-CNRC

NRC Publications Archive
Archives des publications du CNRC

Probing the room temperature deuterium absorption kinetics in nanoscale magnesium based hydrogen storage multilayers using neutron reflectometry, X-ray diffraction, and atomic force microscopy

Kalisvaart, W. P.; Luber, E. J.; Poirier, E.; Harrower, C. T.; Teichert, A.; Wallacher, D.; Grimm, N.; Steitz, R.; Fritzsche, H.; Mitlin, D.

This publication could be one of several versions: author's original, accepted manuscript or the publisher's version. / La version de cette publication peut être l'une des suivantes : la version prépublication de l'auteur, la version acceptée du manuscrit ou la version de l'éditeur.
For the publisher's version, please access the DOI link below./ Pour consulter la version de l'éditeur, utilisez le lien DOI ci-dessous.

Publisher's version / Version de l'éditeur:
https://doi.org/10.1021/jp209296b
The Journal of Physical Chemistry C, 116, 9, pp. 5868-5880, 2012-02-13

NRC Publications Record / Notice d'Archives des publications de CNRC:
https://nrc-publications.canada.ca/eng/view/object/?id=2fc7cda8-89e6-4fe8-98bd-8e67c8cab317
https://publications-cnrc.canada.ca/fra/voir/objet/?id=2fc7cda8-89e6-4fe8-98bd-8e67c8cab317

Access and use of this website and the material on it are subject to the Terms and Conditions set forth at https://nrc-publications.canada.ca/eng/copyright
READ THESE TERMS AND CONDITIONS CAREFULLY BEFORE USING THIS WEBSITE.

L'accès à ce site Web et l'utilisation de son contenu sont assujettis aux conditions présentées dans le site https://publications-cnrc.canada.ca/fra/droits
LISEZ CES CONDITIONS ATTENTIVEMENT AVANT D'UTILISER CE SITE WEB.

Questions? Contact the NRC Publications Archive team at PublicationsArchive-ArchivesPublications@nrc-cnrc.gc.ca. If you wish to email the authors directly, please see the first page of the publication for their contact information.

Vous avez des questions? Nous pouvons vous aider. Pour communiquer directement avec un auteur, consultez la première page de la revue dans laquelle son article a été publié afin de trouver ses coordonnées. Si vous n'arrivez pas à les repérer, communiquez avec nous à PublicationsArchive-ArchivesPublications@nrc-cnrc.gc.ca.

National Research Council Canada | Conseil national de recherches Canada

Canada

THE JOURNAL OF PHYSICAL CHEMISTRY C

Article

pubs.acs.org/JPCC

Probing the Room Temperature Deuterium Absorption Kinetics in Nanoscale Magnesium Based Hydrogen Storage Multilayers Using Neutron Reflectometry, X-ray Diffraction, and Atomic Force Microscopy

W.P. Kalisvaart,*[,†] E.J. Luber,[†] E. Poirier,[‡] C.T. Harrower,[†] A. Teichert,[§] D. Wallacher,[⊥] N. Grimm,[⊥] R. Steitz,[⊥] H. Fritzsche,[∥] and D. Mitlin*[,†]

[†]Chemical and Materials Engineering, University of Alberta and National Research Council Canada/National Institute for Nanotechnology, Edmonton, Alberta, T6G 2M9, Canada

[‡]Optimal Inc., 14492 Sheldon Road, Suite 300, Plymouth Township, Michigan 48170, United States

[§]Forschungs-Neutronenquelle Heinz Maier-Leibnitz, Lichtenbergstraβe 1, 85748 Garching, Germany

[⊥]Helmholtz Zentrum Berlin, Hahn-Meitner-Platz 1, 14109 Berlin, Germany

[∥]National Research Council Canada/Canadian Neutron Beam Centre, Building 459, Chalk River Laboratories, Chalk River, Ontario, K0J 1J0, Canada

Supporting Information

ABSTRACT: Magnesium hydride has high storage capacity (7.6 wt % H) but very slow sorption kinetics. Addition of catalytic phases on the surface as well as alloying with transition metals is known to improve the properties. In this study, the sorption kinetics of a 50-nm Mg layer and Mg-10%Cr-10%V layer, capped with a CrV/Pd bilayer catalyst, are compared using a combination of neutron reflectometry (NR), X-ray diffraction (XRD), and atomic force microscopy to elucidate the effects of alloying on the hydrogen storage properties of Mg at room temperature. From NR it is found that the Cr−V alloyed layer shows both a delay in expansion in the first absorption cycle and a delay in contraction in the first desorption, which indicates a delay in nucleation of MgD_2 and formation of substoichiometric $MgD_{2-\delta}$, respectively. Compared to pure Mg, the kinetics are strongly improved as no blocking MgD_2 layer is formed. XRD showed a strong reduction in the Mg grain size for the Cr−V alloyed layer after one cycle. For pure Mg, the grain size is almost unchanged although the film becomes nanocrystalline in the hydrided state. NR is shown to be highly sensitive to both the deuterium distribution as well as the layer thickness, which makes it a valuable tool for studying reaction mechanisms and quantification of the expansion of both crystalline and amorphous energy storage materials.

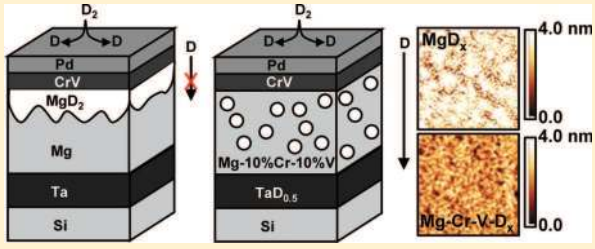

1. INTRODUCTION

MgH_2, because of its high gravimetric hydrogen content (7.6 wt % H), is intensively researched for reversible hydrogen storage systems but suffers from severe kinetic limitations such as extremely low diffusion rate of hydrogen through MgH_2[1−4] and slow hydrogen dissociation on the Mg surface.[5] Until now, the majority of efforts has been directed toward improving the catalytic activity and reducing diffusion limitations. The latter can be achieved by, for instance, confining $Mg(H_2)$ inside a porous matrix[6] or by ball milling of $Mg(H_2)$ with carbon allotropes[7] to keep the particle size small and diffusion distances short. Ball milling has the added advantage of introducing defects[8] and enabling mixing of transition metal (TM) catalysts to promote hydrogen dissociation on the surface.[9−11]

Metastable Mg-TM based films made by sputtering also have greatly enhanced sorption kinetics either by altering the crystal structure of the hydride[12−14] or by forming a Mg-catalyst composite in situ during cycling. Combinations of Mg with 2 transition metals have been shown to have absorption times of 10−20 s and desorption times of 15−20 min at temperatures as low as 200 °C.[15−17] This was ascribed to the formation of a very finely dispersed Mg-TM alloy composite starting from a homogeneous solid solution in the as-deposited state.

The heat of formation of MgH_2 is very negative, $\Delta H_f = -77$ kJ/mol H_2,[18] which means the equilibrium pressure is $\sim 10^{-6}$ bar at 298 K. Because the working pressure is so extremely low, studies of the room temperature behavior of Mg-based materials have focused on electrochemical applications[19] and switchable mirrors/hydrogen sensors.[20,21] Both in bulk materials and thin films, alloy compositions for which the hydride has a metastable face-centered cubic structure[12,14,21] show vastly superior sorption kinetics compared to the

Received: September 26, 2011
Revised: February 9, 2012
Published: February 13, 2012

 © 2012 American Chemical Society

equilibrium rutile structure of MgH_2, which emphasizes the low diffusion rate of hydrogen in rutile MgH_2, especially at low temperatures. Observation of an inverse relation between the charging current, which is the electrochemical equivalent of hydrogenation rate, and hence the nucleation rate, and the total capacity provided indirect evidence for the formation of MgH_2 blocking layers in Pd-capped thin films.[22,23] Similar to high-temperature studies, formation of a composite material of Mg with a secondary phase, improved the storage capacity and reaction kinetics significantly.[24]

The TM alloy particles are generally amorphous or nanocrystalline and are thought to serve as heterogeneous nucleation sites for the hydride and metal phase during absorption and desorption and act as a rapid diffusion path for hydrogen.[15,25] However, direct observation of spatial correlations between the catalytic phase and Mg hydride or Mg metal by, for instance, transmission electron microscopy has many experimental difficulties associated with it such as hydride instability and oxidation under an electron beam,[26] even when cooled to liquid nitrogen temperatures.[8] Therefore, an in situ technique with high spatial resolution is preferable. Neutron reflectometry (NR) is capable of resolving deuterium concentration profiles with nanometer resolution in a direction perpendicular to the substrate.[27,28] From the deuterium penetration depth as a function of time, the deuterium diffusion rate can be evaluated and from the shape of the concentration profiles (e.g., constant across a layer, sharp boundary between reacted and unreacted material, concentration gradients, etc.), information about the nucleation and growth mechanisms can be obtained.

Many of the cosputtered Mg-TM films studied so far show an activation period where the kinetics consistently improve over the first 5−10 cycles. The as-sputtered alloys are metastable, and the alloying elements have separated from Mg after 20 cycles or less at 200 °C.[15] Since phase separation would involve long-range diffusion of metal atoms, this process is expected to proceed much more slowly at room temperature. Mg expands by 32% in volume upon hydrogenation, making the material sensitive to pulverization. Metastable solid solutions in either crystalline or amorphous state may display anomalous behavior in terms of lattice expansion as the concentration of H is increased.[29] A study by Gonzalez et al. of the optical properties of cosputtered Mg−V films showed large differences between the first and subsequent absorption cycles.[30] The biggest optical change was measured at considerably higher pressure in the first cycle. The plateaus also became more sloping in later cycles. Because the measurements were performed in quasi equilibrium, the pressure was increased at ∼3 Pa/min; a sloping "plateau" indicates that the hydrided fraction increases more slowly with time and that absorption has become diffusion-limited, whereas the first cycle may have a different rate-limiting step. Because NR is very sensitive to the layer thickness as well as the deuterium concentration, reflectivity measurements combined with crystallographic data can provide valuable insights into the behavior of these materials at low temperatures.

The present paper presents a comparative NR study between a baseline 50 nm thick Mg layer and a catalyzed Mg-10%Cr-10%V layer covering one complete absorption−desorption cycle at room temperature. Cr and V have already proved to be effective catalysts in combination with Ti and Fe, respectively,[16,17] and preliminary cycling data on Mg−Cr−V showed comparable absorption kinetics to other Mg-TM based alloys.[31] The NR data will be used to study the effects of alloying on the sorption kinetics, more specifically deuterium diffusion. Combining these with data on the evolution of the lattice parameters from X-ray diffraction, the phase separation mechanism will be elucidated. Atomic force microscopy is used to study the behavior of the Pd top layer and as independent verification of the interfacial roughness between the layers as derived from fitting the reflectivity data.

2. EXPERIMENTAL METHODS

The samples were deposited onto 4-in. Si wafers using a RF/DC-magnetron cosputtering system (AJA International). Deposition of the layers was performed sequentially without interruptions and at room temperature in sputter-up configuration while rotating the substrate at ∼0.5 Hz. Sputtering was performed at an Ar pressure of 4 mTorr. Base pressure in the deposition chamber was 5×10^{-8} Torr or lower. Analogous to previous NR studies,[28,32,33] a 10-nm Ta layer was deposited first. Ta is also a hydride-forming element and can thus be used as a "probe" to evaluate the hydrogen (deuterium) penetration rate through the stack. Ta was deposited using RF sputtering at 150 W (1.1 Å/s). Mg was deposited using 100 W (DC) at a rate of ∼2.5 Å/s. Cr and V rates were adjusted to obtain the desired stoichiometry. Pd was deposited at 50 W DC power (1.54 Å/s). A Pd/CrV bilayer catalyst is used rather than a single Pd layer to prevent interdiffusion and avoid clamping effects at the interface with Mg.[34] A schematic representation of the sample configuration is shown in Figure 1.

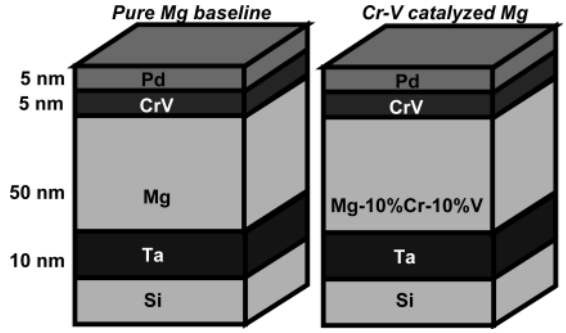

Figure 1. Sample configuration used for all experiments.

Reflectometry measurements on 10 nm Ta/50 nm Mg(10% Cr-10%V)/5 nm CrV/5 nm Pd were performed on the D3 reflectometer at the NRU reactor at Chalk River Laboratories, Chalk River, Ontario, Canada. A 10-nm Ta/50-nm Mg/5-nm Ta/5-nm Pd stack was measured on the V6 horizontal reflectometer at the Helmholz Zentrum in Berlin. Deuterium absorption was performed in situ using an aluminum sample cell and high purity deuterium (99.999%). The reflectivity curves were measured at grazing incidence in specular geometry as a function of the incident angle θ. In this configuration, NR can be treated in way analogous to optical reflectivity. The "neutron index of refraction" n depends on the neutron scattering length b_j of the specific isotope and the number density of scatterers per unit volume N_j according to

$$n^2 = 1 - \frac{\lambda^2}{\pi} N_j b_j \tag{1}$$

where λ is the wavelength of the neutrons, which is 2.37 Å for the D3 reflectometer in Chalk River and 4.66 Å for the V6 in Berlin. The product $N_j b_j$ is also called the scattering length

dx.doi.org/10.1021/jp209296b | J. Phys. Chem. C 2012, 116, 5868−5880

density (SLD) of the layer. Since deuterium has a large coherent scattering length (6.67 fm), deuterium absorption results in a large increase of the SLD in the film.

Total reflection of neutrons occurs up to a critical angle θ_c or scattering vector q_c that can be expressed as

$$q_c = \frac{4\pi}{\lambda}\sin\theta_c = 4\sqrt{\pi Nb} \quad (2)$$

where the product Nb is the total scattering length density in the entire stack. This makes the evolution of q_c over time a good indicator for whether deuterium absorption is still ongoing in the film. Reflectivity data are recorded in the range $0.005 < q < 0.15$. The data acquisition time becomes progressively longer at higher q. The range between $q = 0.02$ and 0.005 was always recorded last so that the measurements around the critical edge always reflect the deuterium content in the film most accurately.

For the in situ reflectometry experiments, the sample chamber was first evacuated and then refilled to the desired deuterium pressure for absorption. Reflectivity curves were measured in the $0.005 < q < 0.05$ range until a steady state had been reached. Then, a complete reflectivity curve up to $q = 0.1$ or 0.15 Å^{-1} was recorded before the pressure was increased further. For desorption, the sample holder was evacuated again and backfilled with 1 bar helium. All absorption measurements were performed at room temperature. For desorption, the Mg-10%Cr-10%V alloy was kept at room temperature, the Mg film was heated to maximum 80 °C.

The reflectivity curves were modeled using Parratt's recursive algorithm,[35] which yields the SLD as a function of depth, either using the Parratt32 program[36] or GenX.[37] The latter has the advantage that it allows for setting upper and lower limits on the values each parameter (SLD, thickness, roughness) can have. Unless explicitly stated otherwise, all fits that will be presented have been obtained using Parratt32. Interfacial roughness is accounted for in this approach. It should be noted here that NR measures the SLD *averaged over the xy plane* for every depth z. Therefore, physical roughness between separate layers can not be distinguished from concentration gradients due to interdiffusion of the metals or slow diffusion of deuterium. For the remainder of this paper, a gradient in the SLD profile will initially be denoted as "roughness," and its most likely origins are discussed later.

From the modeled SLD profiles, the deuterium concentration in each layer can be approximated by[38]

$$C_D = \left[\frac{S_{M+D}}{S_{p=0}}\frac{t_{M+D}}{t_M} - 1\right]\frac{b_M}{b_D} \quad (3)$$

which takes into account the expansion of the layer due to deuterium absorption. S_{M+D} and $S_{p=0}$ are the SLD in the absorbed and deuterium-free layer, respectively, t_{M+D} and t_M are the corresponding thicknesses, and b_M and b_D are the coherent scattering lengths of the metal and deuterium. When there is a gradient in the deuterium concentration, the SLD profile is integrated, and an average SLD is calculated for the layer.

Hydrogenation of the samples used for X-ray diffraction was performed in a Sieverts-type apparatus (HyEnergy PCTPro2000) under identical conditions to those used in the in situ reflectometry measurements. XRD measurements were performed on a Bruker AXS diffractometer (Bruker Discover 8) using Cu Kα radiation monochromatized using a single Göbel mirror. The diffractometer is equipped with a HiStar general area 2-dimensional detection system (GADDs). The sample−detector distance was 15 cm. XRD data were analyzed using the "fityk" program[39] to determine peak positions and integral breadths. The samples used for XRD were deposited at a different time but were identical to the NR samples regarding layer thicknesses and deposition rates. The Scherrer equation[40]

$$D = \frac{\lambda}{B\cos\theta} \quad (4)$$

where λ is the wavelength, B is the intergral breadth of the peak, and θ is the angle, was used to calculate the coherence length D. As the films are highly oriented, generally only 1 reflection/crystallographic direction can be used for determination of the grain size. Instrumental broadening was determined using a LaB_6 standard powder sample with the normal to the sample holder in-plane with the X-ray source and the center of the area detector. Therefore, only peaks visible when the substrate normal is in plane with the source and detector (i.e., $\chi = 0°$) will be used to determine grain sizes. Under these conditions, the instrumental broadening was determined as 0.27°.

Atomic force microscopy (AFM) was performed using a multimode AFM (Veeco Instruments Inc.) operating in tapping mode, equipped with an E-type piezo element. ACTA probes (AppNano) having a nominal radius of 6 nm and resonant frequency of 300 kHz were used.

3. RESULTS AND DISCUSISON

3.1. NR. Parts a and b of Figure 2 show experimental reflectivity curves for the Ta/Mg/CrV/Pd stack in the as-deposited state, after 1 and 20 h exposure to 50 mbar D_2 and in the desorbed state. The SLD profiles obtained from the fit are shown in Figure 2c, also for one more intermediate time step after 5 h. The layer thicknesses and SLDs found from the fits for the as-deposited state together with the theoretical values are summarized in Table 1. The nominal values for the layer thicknesses and SLDs differ by at most ∼10% from the values found in the fit, which supports our measurement and calculation procedures.

The reflectivity curves after 1 and 20 h exposure to 50 mbar D_2 can be fitted quite well over the entire q range from 0.005 to 0.1 Å^{-1} which means that deuterium absorption is slow compared to the time scale of the measurement. Because the scattering length of deuterium (6.67 fm) is larger than that of Mg (5.375 fm), Pd (5.91 fm), Cr (3.635 fm), and V (−0.3824 fm), absorption of deuterium will always increase the SLD in the layer. This is reflected by the clear shift in the critical edge, q_c, toward higher values as predicted by eq 2 and indicated by the arrow in Figure 2b. For the same reason, the SLD depth profiles in Figure 2c can be viewed as a concentration profile of deuterium. At any depth in the film where the SLD has increased compared to the as-deposited state, the deuterium concentration is now larger than zero. The narrow region with high SLD in the top ∼10 nm of the Mg layer in the first hour of absorption is most likely a continuous layer of MgD_2 that has formed directly under the Pd/CrV catalyst.

As was already mentioned, NR measures an average SLD over the xy plane for every depth z. Thus, physical roughness between adjacent layers, which is always modeled as an error function in our case, leads to a gradient in the SLD. Because the root mean square (rms) roughness between the CrV and Mg layers (17.3 Å) and between the deuterated and undeuterated zones within the Mg layer (90.8 Å) is so high, the maximum SLD reaches only 5.5×10^{-6} Å^{-2}, which is lower than the theoretical SLD of MgD_2 (6.11×10^{-6} Å^{-2}). However, when

dx.doi.org/10.1021/jp209296b | J. Phys. Chem. C 2012, 116, 5868−5880

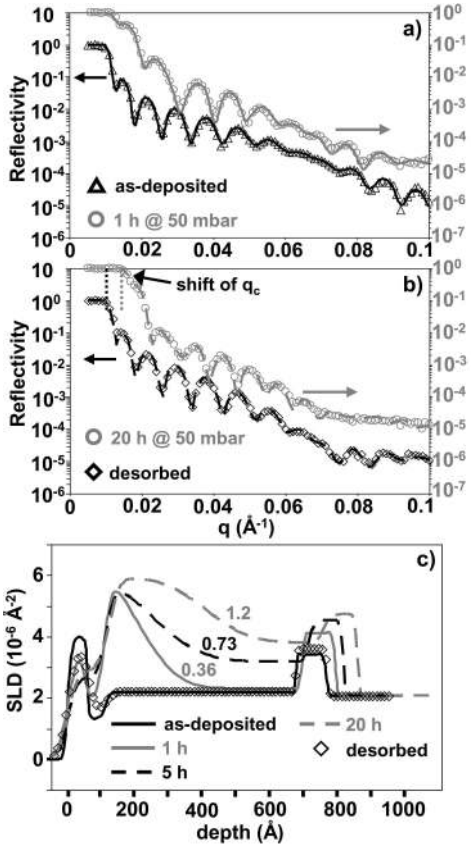

Figure 2. (a) Experimental reflectivity curves of Ta/Mg/CrV/Pd stack in as-deposited state and after 1 h exposure to 50 mbar D_2 at room temperature. Open symbols are data points; solid lines are fits. (b) Experimental reflectivity curves of Ta/Mg/CrV/Pd stack after 20 h exposure to 50 mbar D_2 and after desorption at 80 °C. (c) SLD profiles over the course of absorption and desorption. D/M ratios in the Mg layer are indicated in the figure.

Table 1. Measured and Theoretical SLD and Layer Thicknesses for the Pure Mg Film

	measured SLD (10^{-6} Å^{-2})	theoretical SLD (10^{-6} Å^{-2})	measured thickness (Å)	rms roughness (Å)
		Mg as-deposited		
Pd	3.98	4.02	55.1	9.1
CrV	1.33	1.26	55.0	4.0
Mg	2.18	2.31	555.7	10.9
Ta	3.42	3.85	94.3	0.0
		Mg desorbed		
Pd	3.93	4.02	55.9	23.6
CrV	1.62	1.26	58.7	18.2
Mg	2.21	2.31	554.7	16.1
Ta	3.60	3.85	93.8	5.0

the roughness at the CrV/MgD_2 interface is set to 0, leaving all other parameters the same, the maximum SLD is 6×10^{-6} Å^{-2}, which shows that the very top part of the Mg layer is indeed fully deuterated.

After the initial formation of the MgD_2 layer underneath the catalyst, deuteration progresses only very slowly. From the SLD profiles after 1, 5, and 20 h absorption, the estimated D/M ratios are 0.36, 0.73, and 1.2, respectively. The D/M ratio after 1 h absorption at 50 mbar is calculated from eq 3 as 0.36. This deviates slightly from the value we reported before,[31] but that was based on a narrower q range, $0.005 < q < 0.05$ Å^{-1} (see Figure S1 of Supporting Information for a comparison). The SLD in the Ta layer, after showing a relatively large increase in the first hour from 3.4×10^{-6} to 4.1×10^{-6} Å^{-2} (D/M ~0.25), increases very slowly over the course of the next 19 h, up to a D/M ratio of ~0.4. This illustrates the extremely low hydrogen diffusion rates through $MgD(H)_2$ and the useful role of a hydride-forming layer at the bottom of the stack.

The $Mg(D_2)$ layer thicknesses obtained from the fit show an increase from 555 to 583 Å (deuterated 98.2 Å + undeuterated zone 483.7 Å) corresponding to 4.6% expansion relative to the as-deposited state after 1 h. On the basis of the estimated D/M ratio, 5.6% expansion is expected, which is quite close to the measurement. In the course of absorption, the total thickness of the Mg layer increases to 598 Å at 0.73 D/M and 631 Å at 1.2 D/M where 620 and 662 Å would be expected (the fitting parameters for all reflectivity curves are listed in the Supporting Information). The discrepancy between expected and measured expansion thus seems to increase with time. However, the high interfacial roughness that develops between the layers during the course of absorption introduces some uncertainty in the layer thicknesses.

To desorb the layer, the sample was heated to a maximum of 80 °C. After desorption was complete, the Mg layer has returned to exactly the same thickness as in the as-deposited state (see Figure 2b and Table 1). This is different from the results obtained by Dura et al., who observed no contraction at all upon desorption. Instead, formation of voids was observed between the Mg layer and the Al_2O_3 substrate.[41] The substrate, layer thicknesses, and reaction conditions (temperature, pressure) used were substantially different from ours, which may account for most of the differences in our observations.

The roughness between the catalyst layer and the Mg and CrV layers have decreased down to a point where the catalyst layers are once again distinguishable from one another. This shows the deformation of the $Mg(D_2)$/CrV interface is, for the major part, reversible. Despite that, the interfacial roughnesses are considerably higher than in the as-deposited state. Because the sample was heated, the increased roughness could be due to interdiffusion between Pd and Mg through the CrV layer. From the reflectivity curves in Figure 2, it can be seen that the main effect of increased interfacial roughness is decreased intensity at $q > 0.04$ Å^{-1}. The Ta layer is still slightly expanded and has a slightly higher SLD compared to the as-deposited state, indicating that there is still some deuterium in the layer.

The results obtained at 50 mbar deuterium pressure clearly showed formation of a blocking layer of MgD_2 directly underneath the catalyst bilayer. Formation of blocking layers of $MgH(D)_2$ has been observed before when the driving force for hydrogenation is high.[42] It is therefore interesting to investigate the effects of using a lower absorption pressure. Figure 3 shows the measured reflectivity curves of a 10 nm Ta/50 nm Mg/5 nm Ta/5 nm Pd stack in the as-deposited state and after 2 h 20 min exposure to 20 mbar D_2 at room temperature. For the as-deposited state, the SLDs obtained from the fit are close to the nominal values as shown in Table 2. Exposure to 20 mbar deuterium increases the SLD in both Ta layers is increased compared to the as-deposited state, most notably the top one.

When comparing the SLD profiles in Figure 3b with those in Figure 2c a very interesting observation can be made. The best fit to the reflectivity data is obtained by dividing the Mg layer into three "slabs", each approximately 175 Å wide with ~50 Å

dx.doi.org/10.1021/jp209296b | J. Phys. Chem. C 2012, 116, 5868−5880

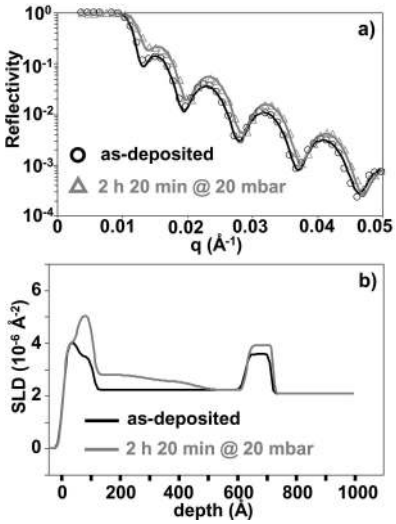

Figure 3. (a) Reflectivity curve and fit for as-deposited 10 nm Ta/50 nm Mg/5 nm Ta/5 nm Pd and after 2 h and 20 min exposure to 20 mbar D_2. (b) SLD profiles for the as-deposited state and after 2 h 20 min exposure to 20 mbar D_2 at room temperature.

Table 2. Model Parameters in As-Deposited State and after 2-Hour 20-Minute Exposure to 20 mbar D_2 (Best Fit) for 10 nm Ta/50 nm Mg/5 nm Ta/5 nm Pd Stack

	measured SLD (10^{-6} Å^{-2})	measured thickness (Å)	rms roughness (Å)
	as-deposited		
Pd	4.03	51.0	10.9
Ta	3.48	52.0	10.0
Mg	2.21	521.7	10.0
Ta	3.57	90.0	10.3
	2 h 20 min at 20 mbar		
Pd	4.00	50.0	10.9
Ta	5.03	53.0	10.0
Mg_1	2.80	178.0	10.0
Mg_2	2.55	175.0	53.5
Mg_3	2.21	175.0	46.2
Ta	3.91	91.5	10.3

rms roughness between each of the slabs. The estimated D/M ratio is approximately 0.13 at this point, and the Mg layer expands slightly to a total thickness of 528 Å. On the basis of the estimated D/M ratio, approximately 2% expansion would be expected up to 532 Å, but the uncertainties in the SLD and layer thicknesses are slightly larger compared to Figure 2 due to the limited data range up to q = 0.05 Å^{-1}. At this lower pressure, a continuous blocking layer of MgD_2 is obviously not formed. The SLD in the top part, directly below the Pd/Ta bilayer catalyst, only reaches 2.80 × 10^{-6} Å^{-2}, which is nowhere near the theoretical SLD of MgD_2. The *penetration depth* of deuterium, on the other hand, is actually greater at lower total deuterium content compared to the situation at 50 mbar. After 2 h and 20 min at 20 mbar, the SLD in the Mg layer is noticeably higher than in the as-deposited state down to a depth of approximately 400 Å, compared to ~320 Å after 1 h at 50 mbar, despite a three times higher deuterium content in the latter case.

These results show that the nucleation rate of MgD_2, especially at the Mg/CrV(Ta) interface is much lower at 20 mbar than at 50 mbar, as expected. Conversely, formation of a blocking layer is avoided at lower pressures. This would be favorable to the kinetics, but the lower driving force decreases the deuteration rate in this case, although an effect from the different bilayer catalysts (CrV/Pd vs Ta/Pd) can not be ruled out. The most important conclusion, however, can be drawn from the shape of the SLD profiles at both pressures. The large gradient in the SLD profiles in Figure 2 and the "steps" in Figure 3 strongly suggest that the grain boundaries in the Mg layer function as rapid diffusion paths for deuterium and preferential nucleation sites for the deuteride. At 20 mbar, MgD_2 seems to nucleate mainly at grain boundaries in the Mg layer, whereas at higher pressures the Mg/CrV interface acts as a preferential nucleation site as well. This is very interesting because transition metal based catalysts in cosputtered films have always been assumed to act as preferential heterogeneous nucleation sites and rapid diffusion paths for hydrogen. After cycling, XRD always showed a fully segregated mixture, but the sorption kinetics show a clear activation period where they become considerably more rapid in the initial 5−10 cycles.[15−17] From a comparison between Mg and Mg-10%Cr-10%V during the first cycle, we should be able to find out more about the origins of this activation period.

Parts a−c of Figure 4 depicts the reflectivity curves and SLD depth profiles obtained in the course of deuterium absorption for Mg-10%Cr-10%V. For the as-deposited state, the layer thicknesses and SLDs obtained from fitting the reflectivity data are summarized in Table 3 and are quite close to the nominal values. Subsequently, deuterium was introduced into the sample cell at a pressure of 10 mbar. Figure 4a shows that after only 10 min, the critical edge has moved to significantly higher q (from 0.01 to ~0.012 Å^{-1}), indicating that the sample has absorbed a considerable amount of deuterium. From the SLD profiles in Figure 4d, it is clear that the SLD in the Ta layer has already increased to its maximum value, 5.5 × 10^{-6} Å^{-2}, at this point in time. The rapid increase in the SLD of the Ta layer shows that, contrary to the pure Mg baseline, deuterium diffusion through the layer is fast. This means that MgD_2 has either not been formed yet or that it does not form as a closed layer as it did in pure Mg.

The SLD in the Mg-10%Cr-10%V layer increases to 3.05 × 10^{-6} Å^{-2} after 10 and 3.94 × 10^{-6} Å^{-2} after 20 min, which corresponds to a D/M ratio of 0.25 and 0.5, respectively. Curiously, the thickness of the layer has not yet increased, despite the fact that Mg undergoes a 32% volume expansion upon transformation to MgD_2. This is immediately obvious from the reflectivity curves as the oscillation periodicity $\Delta q \approx 2\pi/d$, where d is the total thickness of the stack,[27] has not yet changed. A possible explanation for this delay in expansion will be discussed later. Near the critical edge, the fit to the reflectivity curve is not as good as at higher q, as is clearly visible in Figure 4b. As we mentioned in the Experimental section, the data at $0.005 < q < 0.02$ Å^{-1} was always recorded last. When absorption is relatively fast, the fitted reflectivity curve, based on all the data up to 0.05 Å^{-1}, will deviate from the measurement the most around the critical edge. As would be expected during *ab*sorption, the critical edge is at slightly higher q in the experimental data compared to the fit.

Only after 30 min does the layer undergo significant expansion to a total thickness of ~700 Å, as the SLD profile shows. The top 250 Å has reached its maximum SLD value of 5.5 × 10^{-6} Å^{-2} after which the SLD decreases smoothly toward the Ta layer. The presence of a gradient in the SLD means that diffusion of deuterium through the layer has become slower

dx.doi.org/10.1021/jp209296b | J. Phys. Chem. C 2012, 116, 5868−5880

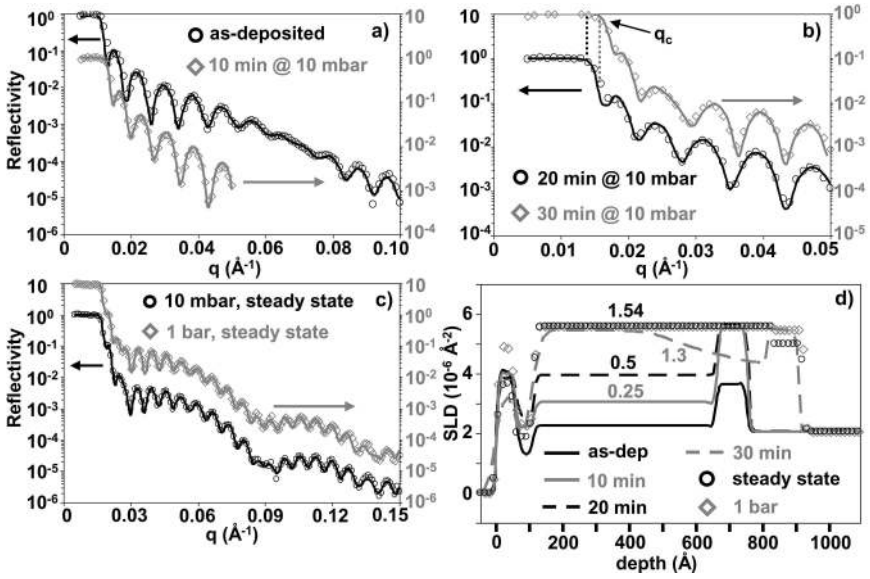

Figure 4. Reflectivity curves (a–c) and corresponding SLD profiles (d) for Mg-10%Cr-10%V in the course of absorption at room temperature. Open symbols are measured data points; solid lines are fits. Estimated D/M ratios are indicated in the SLD depth profiles. The indicated times refer to the exposure time at 10 mbar.

Table 3. Measured and Nominal/Theoretical Layer Thicknesses and Scattering Length Densities of the Different Layers in the As-Depostied Mg-10%Cr-10%V Film

Mg-10%Cr-10%V as-deposited	measured SLD (10^{-6} Å^{-2})	theoretical SLD (10^{-6} Å^{-2})	measured thickness (Å)	nominal thickness (Å)
Pd	4.09	4.02	57.4	50
CrV	1.25	1.26	52.2	50
Mg-10%Cr-10%V	2.25	2.18	553.6	500
Ta	3.65	3.85	93.3	100

Table 4. Measured Layer Thicknesses and Scattering Length Densities of the Different Layers in the Mg-10%Cr-10%V Film in the Saturated State at 10 mbar and 1 bar Deuterium Pressure

Mg-10%Cr-10%V 10 mbar	measured SLD (10^{-6} Å^{-2})	measured thickness (Å)	estimated D/M ratio
Pd	3.67	51.3	0
CrV	1.88	61.0	0.17
Mg-10%Cr-10%V	5.59	718.3	1.54
Ta	5.01	98.6	0.42
Mg-10%Cr-10%V 1 bar	measured SLD (10^{-6} Å^{-2})	measured thickness (Å)	estimated D/M ratio
Pd	4.95	51.3	0.07
CrV	2.27	61.0	0.26
Mg-10%Cr-10%V	5.60	717.8	1.54
Ta	5.48	100.8	0.60

and that MgD_2 has now been formed. The estimated D/M ratio in the Mg–Cr–V layer is 1.3. This shows the absorption rate accelerates past 0.5 D/M, which took 20 min, increasing by 0.8 in only 10 min. A similar acceleration of the absorption rate was found for Mg-10%Cr-10%Fe, also coinciding with the onset of expansion of the layer.[43]

After approximately 1 h, the reflectivity curves showed no more significant changes over time up to q = 0.05 Å^{-1} and absorption was assumed to be complete. Compared to the pure Mg layer, 1.2 D/M over a period of 20 h, absorption is completed much more rapidly in the alloy layer. The reflectivity curves depicted in Figure 4c were recorded over the full q-range between 0.005 and 0.15 Å^{-1} at 10 mbar and 1 bar deuterium pressure, respectively. The influence of the pressure increase on the reflectivity curves is minor but clearly detectable in the range 0.08 < q < 0.11 Å^{-1}. The layer thicknesses and SLDs obtained from the fits are summarized in Table 4, together with the estimated D/M ratios. The final D/M ratio for the Mg-10% Cr-10%V layer is estimated at 1.54, which is close to the theoretical maximum of 1.6, which would correspond to 2 D/Mg. The layer has expanded by 29.6% to a final thickness of ~718 Å. The Ta layer has expanded from 93.3 to 98.6 (10 mbar) and 100.8 Å (1 bar) and has an estimated D/M ratio of 0.42 at 10 mbar and 0.6 at 1 bar. The deuterium content in the Pd and CrV layers remains rather low, with the Pd absorbing 0.07 D/M only when the pressure is increased to 1 bar.

To desorb the sample, the sample holder was first evacuated to below 10^{-2} Torr and refilled with 1 bar He. No heating was applied. After 1 h, the D/M ratio in the catalyst bilayer and the bottom Ta layer has decreased to 0 and 0.35, respectively. For the Mg alloy layer, only a minute decrease, 0.04 D/M, in the deuterium content was found. After 2 h, the situation was effectively unchanged; the reflectivity curve almost completely coincided with the one measured after 1 h.

After 3 h, the reflectivity curve finally started changing. It was difficult to obtain a good fit for the entire data range from 0.005 < q < 0.1 Å^{-1}. Therefore, the SLD profiles in Figure 5c for 3 and 4 h desorption are based on the data up to q = 0.05 Å^{-1}. As can be seen in Figure 5a, the agreement between the measured data and the model is quite good up to 0.085 Å^{-1}, although the simulated curve has consistently slightly lower intensity at 0.05 < q < 0.085 Å^{-1}. Beyond q = 0.085 Å^{-1}, the model starts to deviate from the measured data quite strongly, which shows the top part of the Mg–Cr–V layer started to desorb during this particular measurement. For both measurements after 1 and 3 h, their fitted curves, and for the extrapolation to q > 0.05 Å^{-1} for the fit after 3 h, the oscillation maxima are spaced identically. This means that, despite having desorbed a considerable amount of deuterium, the layer has not contracted yet. The estimated D/M

dx.doi.org/10.1021/jp209296b | J. Phys. Chem. C 2012, 116, 5868–5880

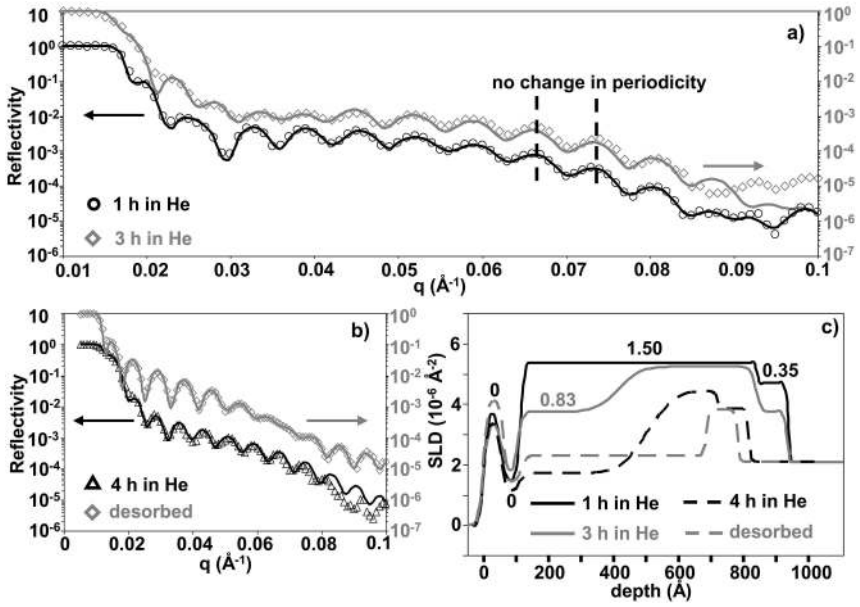

Figure 5. (a) Reflectivity curves of Mg-10%Cr-10%V after 1 and 3 h desorption in He at room temperature. The fit after 3 h is based on data between q = 0.005 and 0.05 Å^{-1} and extrapolated to q = 0.1 Å^{-1}. Note that the oscillations after 1 h, 3 h, and the extrapolated fit all have identical periodicity, showing the layer has not contracted. (b) Reflectivity curves after 4 h desorption and for the fully desorbed state. Same as after 3 h, the only the data between q = 0.005 and 0.05 Å^{-1} is fitted after 4 h. (c) SLD profiles in the course of desorption. D/M ratios after 1 and 3 h in He are indicated in the figure.

ratio in the partially desorbed part of the layer is approximately 0.83.

Between 3 and 4 h, the SLD decreases further throughout the entire layer and the thickness of the Mg-10%Cr-10%V layer now decreases accordingly. When the simulated reflectivity curve based on the SLD profile is extended up to q = 0.1 Å^{-1}, the fit becomes much worse at higher q, both in intensity and oscillation periodicity. This indicates that the layer is desorbing deuterium *and* contracting in thickness, relatively rapidly at this point. Contrary to absorption, there is a relatively sharp boundary between a fully desorbed and partially absorbed region within the Mg alloy layer.

Desorption was completed at room temperature after approximately 6 h. The SLD found for the Mg alloy layer is again very close to that found for the as-deposited state (2.28×10^{-6} Å^{-2}). There is a small, but detectable, residual expansion in the layer of approximately 2.5%. The Ta layer at the bottom remains with a slightly higher SLD and thickness compared to the as-deposited state, most likely due to a small amount of residual deuterium.

The delay in contraction during desorption of the Mg-10%Cr-10%V layer is consistent with previous reports on the existence of a substoichiometric $MgD_{2-\delta}$ phase.[44,45] Schimmel et al. reported detection of $MgD_{1.2}$ with unit cell volume essentially equal (0.5% difference) to stoichiometric MgD_2.[43] For a layer with 80 at % Mg, 1.2 D/Mg would correspond to 0.96 D/M, close to the estimate from the SLD profile. In principle, a decrease in the SLD at constant thickness could also be caused by void formation as observed by Dura et al.,[39] but both the Mg and Mg-10%Cr-10%V layer are close to their original thickness after desorption, which makes it highly unlikely void formation occurred in our experiments.

3.2. X-ray Diffraction. Figure 6a shows the XRD patterns for as-deposited Mg at χ = 0 and 60° and the desorbed Mg film at χ = 0°. For the as-deposited state, the Mg peak positions are at 34.48° for (002) and 36.60° for (101), yielding a = 3.213 and

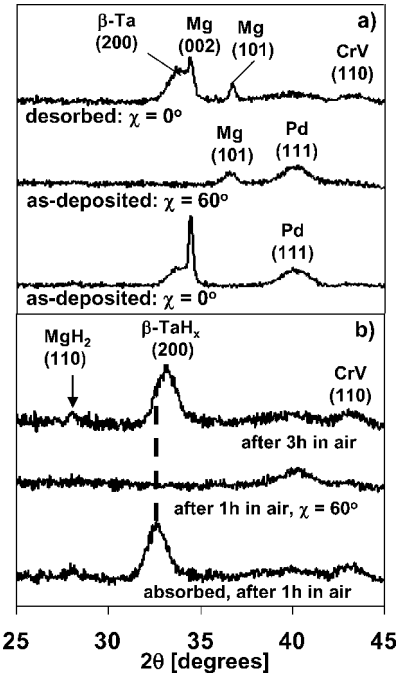

Figure 6. XRD patterns of Mg film (a) as-deposited at χ = 0 and 60° showing both the Mg (002) and (101) reflections and in the desorbed state at χ = 0°. (b) Absorbed Mg film after 1 and 3 h of exposure to air.

c = 5.198 Å and a molar volume of 13.99 cm^3, which is, within the errors, equal to the theoretical value of 14.00 cm^3. The unit cell is, however, slightly distorted compared to bulk Mg. The c/a ratio for the film is 1.618 vs 1.624 for bulk Mg. As seen in Figure 6a, the (200) reflection of the metastable tetragonal β-Ta phase[46] is visible at 33.8° as opposed to the (110) reflection of the equilibrium body-centered cubic Ta phase that is commonly found when the Ta layer is deposited on Pd or Mg (alloy)[15] instead of directly on Si.

dx.doi.org/10.1021/jp209296b | J. Phys. Chem. C 2012, 116, 5868−5880

The film was exposed to 50 mbar H_2 for 20 h identical to the NR measurements, and to 1 bar for another 2 h to ensure complete hydrogenation. Figure 6b, shows the XRD patterns of the hydrogenated film, 1 and 3 h after it has been taken out of the Sieverts machine into ambient air. The only reflections that are clearly visible are the (200) reflection of TaH_x and the (110) reflection of the CrV layer. The TaH_x peak shifts back to higher angles between 1 and 3 h in air, which shows that the film is desorbing relatively rapidly. There is a very small signal at the expected position of the MgH_2, indicated by the arrow, but it barely registers above background level. Apparently, the strong preferential (002) orientation of the as-deposited film (rocking curves are included in Figure S5 of Supporting Information) is completely lost during the transformation to MgD_2. Previous studies found that (002)-oriented Mg thin films transform into (110)-oriented MgH_2,[31,47−49] but most of these studies were performed on much thicker films.[46,47] The study by Higuchi et al. is in particularly good agreement with our results; for Mg thickness of 50 nm and lower, virtually no crystalline MgH_2 was detected.[45]

The NR results showed that at 50 mbar pressure the grain boundaries served as a preferred nucleation site, but that the bulk of the Mg grains were transformed as well, right from the beginning of the absorption process (see Figure 2c). Since the grain boundaries are relatively disordered regions in the material, preferred orientation would be expected to be lost, but for "bulk" transformation a certain orientational relationship would be expected resulting in a clearly detectable preferred orientation for the hydride. Two possible orientational relationships are schematically depicted in Figure 7. In the case of Mg (002)||

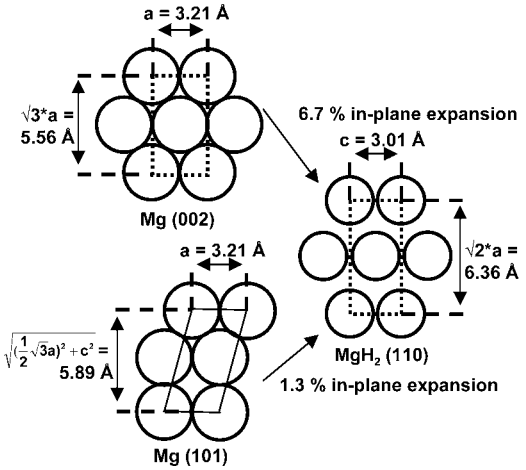

Figure 7. Schematic representation of transformation of Mg metal to Mg hydride phase.

MgH_2 (110) commonly found for thin films,[44−46] the *a* axis of Mg contracts from 3.21 Å to 3.01 Å forming the *c* axis of MgH_2. The other side of the dashed rectangle elongates from $2d_{Mg(100)}$ to $2d_{MgH_2(110)}$, increasing its area by 6.7%. On the basis of the amount of "mismatch", a very different orientational relation would be expected. As illustrated in the bottom part of Figure 7, MgH_2 (110) plane is expanded only 1.3% compared to the Mg (101) plane. However, due to the preferential (002) orientation of the film, the amount of expansion in the *substrate* plane would still be more than 10%. Because the film is constrained by the Si substrate, any expansion is very hard to accommodate except in the *z* direction. Thus, formation of well-crystallized, well-oriented MgH_2 is very unlikely and clearly did not happen here. The MgH_2 (110) reflection was observed neither at $\chi = 0$ nor $\chi = 60°$ (see Figure 6b), which is the angle between the Mg (002) and (101) planes. This could also explain the high interfacial roughness between the $Mg(D_2)$ and CrV layer as expansion has to somehow be accommodated out-of-plane.

After complete desorption, both the Mg (002) and (101) reflections are visible at $\chi = 0°$ at the same 2θ values as for the as-deposited film. Remarkably, the integral breadth of the (002) reflection increases only very slightly from 0.35° for the as-deposited film, which is close to the instrumental broadening determined for the LaB_6 standard, to 0.38° for the desorbed film. The coherence length calculated for the (002) reflection after correction for instrumental effects is 412 Å for the as-deposited and 345 Å for the cycled state. After desorption, both the Mg (002) and Mg (101) reflection at $\chi = 0°$ have the same integral breath of 0.38°. The Pd (111) reflection is only visible for the as-deposited state. Apparently, its preferential orientation is lost upon hydrogenation/dehydrogenation, making such an extremely thin layer hard to detect.

Figure 8 shows the XRD patterns at $\chi = 0°$ of the as-deposited, hydrided, and desorbed Mg-10%Cr-10%V film (a) at

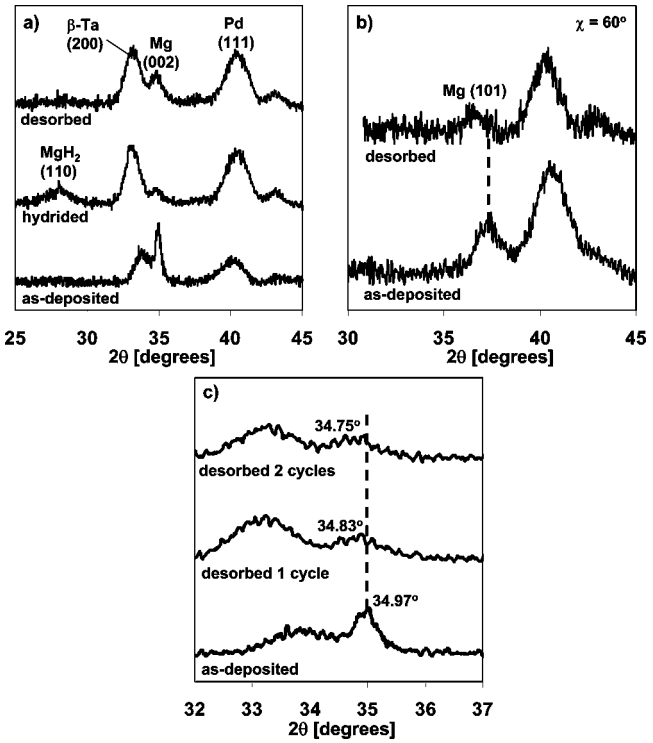

Figure 8. XRD patterns of Mg-10%Cr-10%V. (a) As-deposited, hydrided, and desorbed states at $\chi = 0°$. (b) As-deposited and desorbed states at $\chi = 60°$ shwoing the (101) reflection. (c) Magnification of Ta (200) and Mg (002) reflections for as-deposited and desorbed state after 1 and 2 cycles.

$\chi = 60°$ for the as-deposited and desorbed state (b) and a magnification of the 32−37° 2θ range highlighting changes in the Mg (002) reflection (Figure 8c). The (002) reflection is at 34.97° in the as-deposited state, which means $c = 5.127$ Å. The (101) reflection is detected at 37.05° at $\chi = 60°$, from which $a = 3.177$ Å and the molar volume is 13.49 cm^3. This shows that in as-deposited Mg-10%Cr-10%V, the unit cell volume is contracted by 3.6% compared to Mg, indicating that Cr and V do dissolve in the Mg lattice. An ideal solid solution

dx.doi.org/10.1021/jp209296b | J. Phys. Chem. C 2012, 116, 5868−5880

would have a molar volume of 12.45 cm^3 according to Végard's law, which is ~8% smaller than the measured value. This is in agreement with previous studies on binary sputtered thin films of Mg−V and Mg−Cr, both of which also showed a substantial positive deviation from Végard's law.[30,50]

Not only does the molar volume of the Mg-10%Cr-10%V film deviate positively from Végard's law, it is also substantially larger than the average molar volume of a segregated metal mixture (weighted by at %) of 12.75 cm^3. The lack of expansion up to 0.5 D/M that was observed in the NR experiments can potentially be explained based on this observation. Segregation of the Cr and V could shrink the layer by ~6%, assuming all Cr and V are dissolved in Mg in the as-deposited film. On the basis of the aforementioned studies on Mg−V[30] and Mg−Cr,[48] this is a reasonable assumption. However, to fully compensate for the expansion due to formation of MgD_2, *all* Cr and V would have to separate from Mg, but at 0.5 D/M the layer is only 30% deuterated.

For Mg, the α-solid solution region is very narrow and extends only up to ~0.001 H/M even at 300 °C.[51] DFT calculations by Tao et al. on Mg and Ti showed strongly positive enthalpy of solution for the first 0.25 H/Mg,[52] in agreement with earlier experimental data,[18] which means it is energetically more favorable to form MgH_2 already at very low hydrogen content. Alloying might alter the enthalpy of solution in the α-solid solution region, but this is, to the authors' knowledge, largely unexplored territory in theoretical studies. However, given the low hydrogen affinity of Cr, it is unlikely that partial substitution of Mg for Cr and V would lead to a wider solid solution region at low D-content.

The (110) reflection of MgD_2 is at its theoretical position for the hydrogenated alloy film, at 28.0 ° (see Figure 8). This suggests no Cr or V was incorporated in the hydride structure, though it should be noted that the (110) peak position gives no information on the *c*-axis. Substitution of Mg with 3d transition metals tends to strongly destabilize the rutile MgH_2 structure as theoretical studies have shown for 20 at % substitution of Mg for Cu, Ni, Fe, and Ti,[53] although Cr and V were not calculated. In view of the above, the most likely explanation for the alloy's behavior is that nucleation of MgD_2 is delayed while dissolution of the first 0.5 D/M induces segregation of the Cr and V. The aforementioned study by Tao et al. predicts a moderate expansion of ~5.5% when the tetrahedral sites are filled up to 0.5 H/M in hexagonal close-packed (hcp) Mg,[50] which is within the range that can be compensated by phase segregation. When the Cr and V concentration becomes low enough, the deuteride can finally be formed and will do so throughout the entire layer.

A combined electrochemical hydrogenation/X-ray diffraction experiment such as the one performed by Vermeulen et al. on Mg−Ti cosputtered thin films[54] could potentially clarify the phase segregation process further. Electrochemistry has the big advantage that hydrogenation is quantitative (current multiplied by time) and can be interrupted at will during diffraction measurements, which is not possible for a gas-absorption experiment this far from equilibrium. This would allow for quantitative determination of the relative amounts of hcp Mg and rutile MgH_2 phase and peak positions at a known H/M ratio. This has only been done for binary Mg−Ti so far but could potentially be used to study any Mg-Transition Metal catalyst combination.

Upon exposure to air, the film starts to desorb fairly quickly and a Mg metal peak is clearly visible at 34.83° as well as the hydride peak. Remarkably, the (002) reflection has not shifted back to the theoretical position of Mg after desorption but instead has only shifted by 0.14° compared to the as-deposited state. The (101) peak on the other hand, has shifted considerably toward lower angles at 36.59° (see Figure 8b). The *a* and *c* parameters are now calculated as 3.223 and 5.148 Å, respectively, and the molar volume of the Mg(CrV) phase as 13.95 cm^3.

The c/a ratio for the Mg layer is 1.618, whereas for the Mg-10%Cr-10%V layer it is 1.613 and 1.597 in the as-deposited and cycled states, respectively, which shows the unit cell is distorted for the cycled state. This, combined with the still slightly decreased molar volume, suggests the alloy is not yet fully phase segregated after the first cycle. When the film is subjected to a second, identical cycle, the (002) reflection shifts further toward smaller angles and is now located at 34.75 ° (Figure 8c). The *c*-axis is now 5.159 Å, which is still not entirely identical to the Mg film (5.198 Å). This agrees well with the results obtained by Gonzalez et al., where the films did not reach their final equilibrium state for at least 7 cycles as evidenced by significant changes in the films' optical properties at comparable alloying levels of V.[30] The intensity of the (101) reflection was now too low to be detected reliably.

It is obvious from the width of the Mg (002) reflection in Figure 8 that absorption/desorption cycling reduces the grain size considerably. The integral breadth of the (002) peak is 0.69° in the as-deposited state from which a grain size of 232 Å is calculated after correction for instrumental broadening. Hydrogenation reduces the grain size considerably, as evidenced by the significant broadening of the MgH_2 (110) reflection with respect to the Mg (002) in the as-deposited state. The grain size calculated from the Scherrer equation is now approximately 50 Å. After one complete absorption/desorption cycle, the grain size calculated from the integral breadth of the Mg (002) peak has decreased by a factor 3 compared to the as-deposited state to 71 Å and decreases further down to 58 Å after the second cycle.

These results show that hydrogenation-induced dealloying of the Cr and V from Mg in the first few cycles greatly refines the microstructure compared to pure Mg and this is most likely the reason for the fast kinetics commonly observed in Mg-TM composites during prolonged cycling. Hydrogenation is also much faster compared to pure Mg during the first cycle, due to a delay in the nucleation of MgD_2 as long as phase segregation is still in progress and the fact that hydrogen diffusion through Mg metal is much faster than through MgD_2.[49] The XRD results show that phase segregation is almost completed after the first cycle although multiple cycles are usually needed before the properties of the film reach a steady state.[30] In view of the above, NR measurements during the second and later deuteration cycles of a Mg-10%Cr-10%V film could prove very interesting. Expansion of the film should also start immediately as phase segregation can no longer compensate. Immediate formation of MgD_2 could lead to concentration gradients across the film, although the kinetics should still be at least as fast as in the first cycle.

3.3. AFM. Atomic force microscopy provides an independent measurement of (surface) roughness and can thus be used to validate the assumption of strongly increased interfacial roughness between the layers in the SLD profiles in Figure 2. Figure 9 shows AFM micrographs of the Mg and Mg-10%Cr-10%V films in the as-deposited and hydrogenated state. The top surface of the Pd is very smooth for the as-deposited film with an rms roughness of only 5 Å. In the hydrided state, the

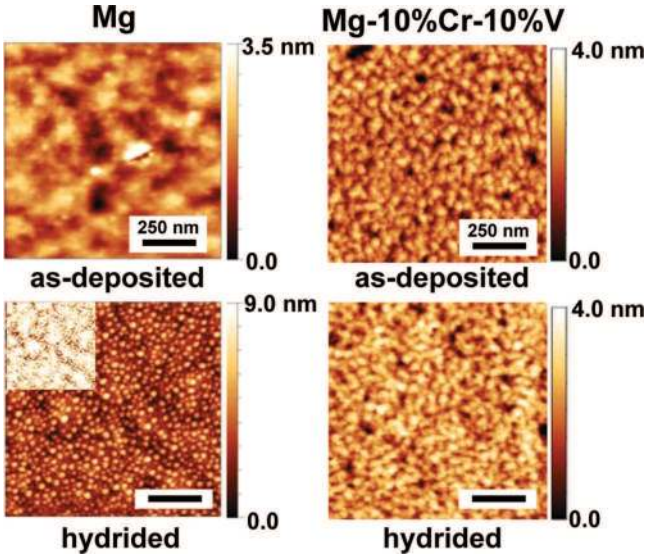

Figure 9. AFM micrographs of Ta/Mg/CrV/Pd and Ta/Mg-10%Cr-10%V/CrV/Pd in the as-deposited and hydrogenated state. The Ta/Mg/CrV/Pd was hydrogenated at 50 mbar for 14 h and Ta/Mg-10% Cr-10%V/CrV/Pd at 10 mbar for 20 h. The inset shows the micrograph of the hydrided film on the same brightness scale as the as-deposited state for Ta/Mg/CrV/Pd.

Pd layer looks as though it has broken up into small particles of approximately 20 nm in diameter. The measured rms roughness has increased by more than a factor of 2 to 13 Å. However, for a completely dewetted layer, one would expect to find a value for the roughness on the order of the original layer thickness, i.e., ∼50 Å. AFM will always underestimate the roughness due to tip dilation effects. In fact, the Pd particles are so closely spaced that the relatively large radius of the AFM tip (6 nm) will almost certainly lead to a large underestimation of the roughness, especially for the hydrided sample. Thus, the increased *surface* roughness found from the NR data is predominantly caused by break-up of the Pd layer into small particles.

The inset shows the hydrided state on the same color scale as the as-deposited state. Much bigger areas than just the Pd particles have significantly increased in brightness, which means the roughness also increases on larger length scales. These AFM results are in good agreement with the reflectivity data, where the roughness of the Pd surface was seen to increase much more strongly and quickly than that of the CrV/Pd and Mg/CrV interfaces and only the latter partially "recover" upon desorption.

For the Mg-10%Cr-10%V film, the rms roughness for the as-deposited state is 5.8 and 6.1 Å for the hydrogenated state. Contrary to the pure Mg film, the roughness found in the AFM measurements does not increase significantly upon hydrogenation. From fitting the reflectivity data, an increase in roughness of the top of the Pd layer of almost a factor 2, from 4.0 to 7.2 Å in the fully hydrogenated state, was obtained. However, when the interfacial roughness is less than 5 Å, the exact value has little influence on the quality of the fit to the reflectivity data. (See Figure S2 of Supporting Information.)

3.4. Simulations. Potentially, there may be multiple SLD profiles that, when used as input for a simulation, generate almost identical reflectivity curves. Conversely, from fitting the experimental reflectivity curves, more than one SLD profile may be generated that produces an equally good fit. It is therefore useful to consider which alternative SLD profiles would describe the reflectivity data equally well, especially considering all the data presented until now. It was mentioned before that the oscillation periodicity is inversely proportional to the layer thickness. Thus, the bilayer catalyst and Ta layers produce oscillations with a periodicity $\Delta q = 2\pi/d$ of approximately 0.12 and 0.06 $Å^{-1}$, respectively, which are "superimposed" upon the reflectivity curve. For instance, in the data at saturation for Mg-10%Cr-10%V in Figure 4c, the underlying oscillation due to the Ta layer can be clearly discerned. However, in all our other measurements, the recorded range in q was always narrower than 0.12 $Å^{-1}$ and during absorption of Mg-10%Cr-10%V it was even shorter than 0.06 $Å^{-1}$. Therefore, it is worthwhile to test the sensitivity of the fit to changes in the SLD of the catalyst and Ta layers. We will present such an analysis for Mg-10%Cr-10%V after 10 min absorption, because it had the narrowest data range and therefore, potentially, the highest degree of uncertainty.

When comparing the results in Figures 4 with those in Figure 2, we can see that the most obvious factors setting the Mg-10%Cr-10%V alloy layer apart from pure Mg are the absence of a blocking layer and the fast, complete deuteration of the Ta layer at the bottom. As shown in parts a and b of Figure 10, the reflectivity data cannot be fitted without increasing the SLD in the Ta and/or the catalyst bilayer. Even when the Pd and CrV layers are assumed to have the same SLD as at 1 bar (see Figure 4d), leaving the SLD in the Ta layer unchanged with respect to the as-deposited state produces a very poor fit. The entire curve is shifted down, and the amplitude of the oscillations is much lower with respect to the experimental data. Optimization of the fit produced an SLD of 5.11×10^{-6} $Å^{-2}$ for the Ta layer, close to the final value at saturation. Even when the D/M ratios were fixed at ∼0.5 (using GenX, the minimum values for the SLD were set at 5.8 and 3.0×10^{-6} $Å^{-2}$ for Pd and CrV, respectively), the optimized value for the SLD in Ta is 4.2×10^{-6} $Å^{-2}$, which is still substantially higher than the value for the as-deposited state (see parts c and d of Figure 10). However, the high roughness on top of the Pd that has to be assumed to fit the oscillation minimum at $q = 0.043$ $Å^{-1}$ properly, strongly disagrees with the AFM measurements in Figure 9. Furthermore, the D/M ratios that were assumed are not very realistic. It is known that for extremely thin Pd layers, i.e., below 10 nm, the solubility of hydrogen at moderate pressures decreases drastically and a maximum D/M ratio of 0.3 was found, even at temperatures as low as 243 K.[55] For CrV, 0.5 D/M, or 1 D/Vanadium, should also be regarded as the absolute maximum at these low pressures since even for pure vanadium the VD-VD_2 transformation occurs above 1 bar at room temperature.[56] Furthermore, the Pd (111) reflection in the XRD patterns in Figure 8 is practically unaffected by hydrogenation/dehydrogenation in terms of intensity and width, indicating that the Pd layer is relatively inert. The equilibrium pressure for formation of $Ta_2D(H)$ is far (∼6 orders of magnitude) below 10 mbar;[56] so in absence of any diffusion barriers in the Mg alloy layer, there is no reason why the Ta layer would not fully transform immediately once the deuterium concentration starts to increase. Therefore, we can conclude that there is some uncertainty in the SLD of the catalyst and Ta layers when the reflectivity data are considered in isolation, but combined with the XRD and AFM measurements and available data from literature, we find that the alternatives to our original best fit either produce unsatisfactory fits or are not physically plausible. A similar analysis for the pure Mg baseline is included in Figure S4 of the Supporting Information.

dx.doi.org/10.1021/jp209296b | J. Phys. Chem. C 2012, 116, 5868−5880

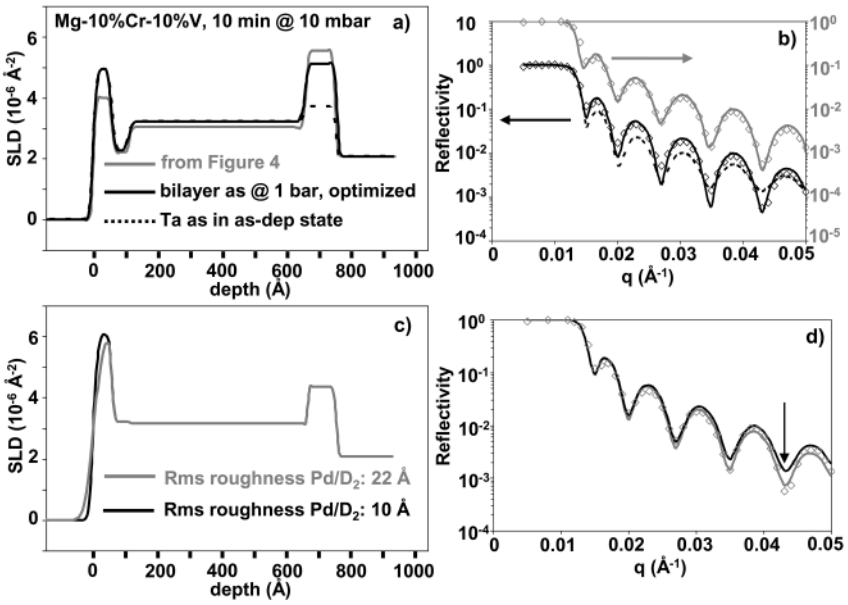

Figure 10. Sensitivity analysis for Mg-10%Cr-10%V after 10 min absorption at 10 mbar to changes in the SLD in the Pd, CrV, and Ta layers. (a) SLD profiles corresponding to the "best fit" from Figure 4 and with increased SLD in the Pd and CrV layers to the levels found at 1 bar with SLD in the Ta layer optimized as well as unchanged with respect to the as-deposited state. (b) Reflectivity curves simulated using the SLD profiles in part a. (c) SLD profiles with Pd and CrV at their theoretical maximum D/M ratios for two different rms roughnesses on top of Pd. (d)Simulated reflectivity curves using SLD profiles from part c.

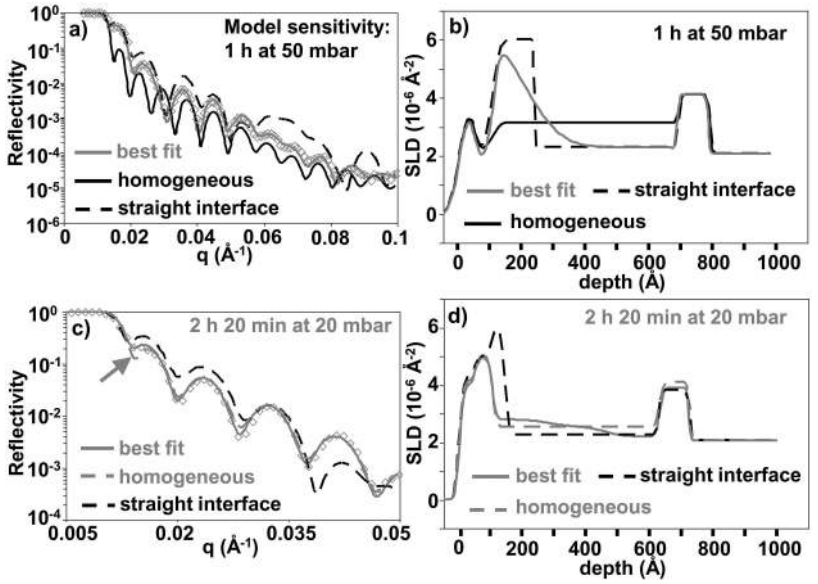

Figure 11. Comparison of experimental data on pure Mg film at 50 (a and b) and 20 mbar (c and d) pressure with simulated reflectivity curves based on other plausible SLD profiles.

In Figure 11, the sensitivity of the reflectivity curves to changes in the deuterium concentration profile inside the Mg layer, rather than the Ta and catalyst layers, is investigated. A comparison between the experimental reflectivity curve and best fit of the Mg film after 1 h at 50 mbar and simulations using different deuterium concentration profiles is shown in parts a and b of Figure 11. The D/M ratio is always the same as in the best fit to the experimental data (0.36 D/M). It is clear that the "step"-like feature at normalized intensity ~0.5 in Figure 11a is unique to a situation where there is clear divide within the Mg layer between a region with high and low D-content as it is absent in the reflectivity curve simulated with a constant SLD across the Mg layer. This shows that the deuteration behavior of the Mg and Mg-10%Cr-10%V, i.e., a flat concentration profile vs a large gradient/blocking layer, are readily distinguished from one another using *only* the reflectivity data. The differences between a SLD gradient and a straight interface between MgD_2 and Mg are also quite substantial especially at $q > 0.055$ Å^{-1}. Even at much lower deuterium content, 0.13 D/M, such as after 2 h and 20 min at 20 mbar from Figure 3, the difference between the "best fit" and the simulation for a straight interface is quite clear as can be seen in parts c and d of Figure 11. The difference between the best fit and a constant SLD across the Mg layer is now very small, which lends further support to our earlier reasoning about the grain boundaries acting as rapid diffusion paths for deuterium.

dx.doi.org/10.1021/jp209296b | J. Phys. Chem. C 2012, 116, 5868−5880

The simulations show that the reflectivity curve is quite sensitive to the deuterium distribution which makes NR, combined with its high sensitivity to the layer thickness, an excellent tool to study amorphous materials such as $Mg_{50}Ni_{50}$[29] and $Mg_{85}Ni_{15}$[57,58] where crystallographic information is not available. As Mg and Ni have negative heat of mixing, contrary to Mg and (Cr)V, the amorphous structure may be quite stable, even during deuterium absorption. Changes in the SLD profile during absorption as cycling progresses, e.g., homogeneous vs a gradient, indicative of crystalline MgD_2, combined with changes in the amount and onset of expansion could detect phase segregation long before diffraction techniques can. Furthermore, there is no reason investigations should be limited to hydrogen storage materials. Degradation mechanisms in (amorphous) Li-storage materials[59] are equally important and could be studied using the same array of experimental techniques we have used here.

4. CONCLUSIONS

The effect of alloying Mg with transition metals on hydriding kinetics was studied with NR by contrasting a pure Mg baseline with a Mg-10%Cr-10%V alloy. For the Mg baseline at 50 mbar pressure, a blocking layer of MgD_2 is immediately formed underneath the bilayer catalyst, and a gradient in the SLD develops across the layer, most likely due to faster deuterium penetration through grain boundaries. At 20 mbar pressure, the overall deuteration rate is lower, but deuterium penetrates deeper into the layer as no continuous blocking layer is formed. These results underline the poor diffusivity of hydrogen through bulk MgH_2 as compared to diffusion through grain boundaries. The Mg film completely loses its preferential orientation in the hydrided state and appears X-ray amorphous, which is likely due to the large mismatch between the Mg and MgH_2 lattice. The Mg grain size undergoes only minor refinement by ~20% between the as-deposited and desorbed state.

For the Mg-10%Cr-10%V alloy, the reaction sequence during the first absorption has been elucidated by combining NR and XRD data. First, deuterium absorption induces segregation of Cr and V from Mg up to a D/M ratio of 0.5. The material shows solid-solution behavior for deuterium at this stage. Because the as-deposited film has a higher molar volume than a segregated mixture, expansion of the Mg lattice due to deuterium dissolution is compensated by segregation of the Cr and V resulting in zero expansion. Finally, when the Cr and V content becomes low enough, the deuteride nucleates throughout the entire layer, avoiding the formation of a blocking layer. The segregated CrV phase subsequently acts as a rapid diffusion path enabling rapid deuteration up to the fully absorbed state, although a small concentration gradient was apparent at the very end (1.3−1.54 D/M). This explains the vastly improved sorption kinetics of Cr−V catalyzed Mg as compared to baseline Mg. Complete absorption takes place at 10 mbar within 1 h, compared to >20 h at 50 mbar for pure Mg.

After the first cycle, the Cr and V are almost completely segregated from Mg as the XRD patterns showed. The unit cell volume and c/a ratio are still slightly smaller than those of Mg. Even after the second cycle, the (002) reflection is still shifted with respect to pure Mg. The microstructure of the alloy film undergoes considerable refinement as evidenced by the strongly diminished Mg grain size and preferential orientation after one absorption/desorption cycle. Studying Mg−Cr−V alloy films over multiple absorption/desorption cycles will be highly interesting as the delay in expansion should diminish at lower CrV content, but fast kinetics should be preserved as the separated CrV phase can act as a rapid diffusion path. This will be subject of future work.

The simulations, combined with the experimental NR data, show that different transformation mechanisms can be readily distinguished from one another. Furthermore, the high sensitivity of the reflectivity curves to changes in the SLD and layer thickness make NR a very attractive technique to study amorphous materials, for which volume expansion is very difficult to quantify by any other means.

■ ASSOCIATED CONTENT

Ⓢ Supporting Information

All parameters corresponding to the "best fits" to the experimental reflectivity curves are included in tabular form as well as the parameters used in simulations. A comparison between Figure 2 and previously published data is also shown. The sensitivity of reflectivity curves to changes in the interfacial roughness, the SLD in the Mg-10%Cr-10%V layer, and the SLD in the bilayer catalyst and Ta layers are also analyzed extensively. The evolution of the rocking curves of the Mg (002) and (101) and MgH_2 (110) reflections during the first cycle is also included. This material is available free of charge via the Internet at http://pubs.acs.org.

■ AUTHOR INFORMATION

Corresponding Author

*Phone: +1-780-850-2678 (W.P.K.); +1-780-492-1542 (D.M.). Fax: +1-780-492-2881 (W.P.K.); +1-780-492-2881 (D.M.). E-mail: pkalisvaart@gmail.com (W.P.K.); dmitlin@ualberta.ca (D.M.).

Notes

The authors declare no competing financial interest.

■ ACKNOWLEDGMENTS

The research presented herein is made possible by a reflectometer jointly funded by Canada Foundation for Innovation (CFI), Ontario Innovation Trust (OIT), Ontario Research Fund (ORF), and the National Research Council Canada (NRC).

■ REFERENCES

(1) Corey, R. L.; Ivancic, T. M.; Shane, D. T.; Carl, E. A.; Bowman, R. C. Jr.; Bellosta von Colbe, J. M.; Dornheim, M.; Bormann, R.; Huot, J.; Zidan, R.; Stowe, A. C.; Conradi, M. S. *J. Phys. Chem. C* **2008**, *112*, 19784.

(2) Hao, S.; Sholl, D. S. *Appl. Phys. Lett.* **2008**, *93*, 251901.

(3) Conradi, M. S.; Mendenhall, M. P.; Ivancic, T. J.; Carl, E. A.; Browning, C. D.; Notten, P. H. L.; Kalisvaart, W. P.; Magusin, P. C. M. M.; Bowman, R. C. jr.; Wang, S. J.; Adolphi, N. L. *J. Alloy. Compd.* **2007**, *446−447*, 499.

(4) Tao, S. X.; Kalisvaart, W. P.; Danaie, M.; Mitlin, D.; Notten, P. H. L.; van Santen, R. A.; Jansen, A. P. J *Int J. Hydrogen Energ.* **2011**, *36*, 11802.

(5) Banerjee, S.; Pillai, C. G. S.; Majumder, C. *J. Chem. Phys.* **2008**, *129*, 174703.

(6) Adelheim, P.; de Jongh, P. E. *J. Mater. Chem.* **2011**, *21*, 2417.

(7) Amirkhiz, B. S.; Danaie, M.; Barnes, M.; Simard, B.; Mitlin, D. *J. Phys. Chem. C* **2010**, *114*, 3265.

(8) Danaie, M.; Tao, S. X.; Kalisvaart, W. P.; Mitlin, D. *Acta Mater.* **2010**, *58*, 3162.

(9) Zhang, J.; Cuevas, F.; Zaïdi, W.; Bonnet, J.-P.; Aymard, L.; Bobet, J.-L.; Latroche, M. *J. Phys. Chem. C* **2011**, *115*, 4971.

(10) Yu, X. B.; Guo, Y. H.; Yang, H.; Wu, Z.; Grant, D. M.; Walker, G. S. *J. Phys. Chem. C* **2009**, *113*, 5324.

(11) Agarwal, S.; Aurora, A.; Jain, A.; Jain, I. P.; Montone, A. *Int. J. Hydrogen Energ.* **2009**, *34*, 9157.
(12) Kalisvaart, W. P.; Niessen, R. A. H.; Notten, P. H. L. *J. Alloy. Compd.* **2006**, *417*, 280.
(13) Srinivasan, S.; Magusin, P. C. M. M.; van Santen, R. A.; Notten, P. H. L.; Schreuders, H.; Dam, B. *J. Phys. Chem. C* **2011**, *115*, 288.
(14) Vermeulen, P.; Graat, P. C. J.; Wondergem, H. J.; Notten, P. H. L. *Int. J. Hydrogen Energy* **2008**, *33*, 5646.
(15) Kalisvaart, W. P.; Harrower, C. T.; Haagsma, J.; Zahiri, B.; Luber, E. J.; Ophus, C.; Poirier, E.; Fritzsche, H.; Mitlin, D. *Int. J. Hydrogen Energy* **2010**, *35*, 2091.
(16) Zahiri, B.; Amirkhiz, B. S.; Danaie, M.; Mitlin, D. *Appl. Phys. Lett.* **2010**, *96*, 013108.
(17) Zahiri, B.; Amirkhiz, B. S.; Mitlin, D. *Appl. Phys. Lett.* **2010**, *97*, 083106.
(18) Griessen, R. P.; Riesterer, T. Heat of formation models. In *Hydrogen in intermetallic compounds I: electronic, thermodynamic, and crystallographic properties, preparation*; Schlapbach, L., Ed.; Springer, 1988; pp 219−284.
(19) Notten, P. H. L.; Latroche, M. Nickel-Metal Hydride Batteries: a succesful Application of Metal Hydrides. In *Encyclopedia of Electrochemical Power Sources*; Garche, J.; Dyer, C.; Moseley, P.; Ogumi, Z.; Rand, D.; Scrosati, B., Eds.; Amsterdam: Elsevier, 2009; Vol. 4, pp 502−521.
(20) Anders, A.; Slack, J. L.; Richardson, J. T. *Thin Solid Films* **2008**, *517*, 1021.
(21) Slaman, M.; Dam, B.; Pasturel, M.; Borsa, D. M.; Schreuders, H.; Rector, J. H.; Griessen, R. *Sensors Actuators, B* **2007**, *123*, 538.
(22) Vermeulen, P.; Niessen, R. A. H.; Notten, P. H. L. *Electrochem. Commun.* **2006**, *8*, 27.
(23) Vermeulen, P.; Ledovskikh, A.; Danilov, D.; Notten, P. H. L. *Acta Mater.* **2009**, *57*, 4967.
(24) Kalisvaart, W. P.; Notten, P. H. L. *J. Mater. Res.* **2008**, *23*, 2179.
(25) Hao, S. *Appl. Phys. Lett.* **2010**, *97*, 111905.
(26) Friedrichs, O.; Sanchez-Lopez, J. C.; Lopez-Cartes, C.; Dornheim, M.; Klassen, T.; Bormann, R.; Fernandez, A. *Appl. Surf. Sci.* **2006**, *252*, 2334.
(27) Zhou, X. L.; Chen, S. H. *Phys. Reports* **1995**, *257*, 223.
(28) Harrower, C. T.; Poirier, E.; Fritzsche, H.; Kalisvaart, P.; Satija, S.; Akgun, B.; Mitlin, D. *Int. J. Hydrogen Energ.* **2010**, *35*, 10343.
(29) Ruggeri, S.; Roué, L. *J. Power Sources* **2003**, *117*, 260.
(30) Gonzalez-Silveire, M.; Gremaud, R.; Balid, A.; Schreauders, H.; Dam, B.; Griessen, R. *Int. J. Hydrogen Energy* **2010**, *35*, 6959.
(31) Kalisvaart, W. P.; Luber, E. J.; Fritzsche, H.; Mitlin, D. *Chem. Commun.* **2011**, *47*, 4294.
(32) Fritzsche, H.; Ophus, C.; Harrower, C. T.; Luber, E.; Mitlin, D. *Appl. Phys. Lett.* **2009**, *94*, 241901.
(33) Fritzsche, H.; Saoudi, M.; Haagsma, J.; Ophus, C.; Luber, E.; Harrower, C. T.; Mitlin, D. *Appl. Phys. Lett.* **2008**, *92*, 121917.
(34) Baldi, A.; Gonzalez-Silveira, M.; Palmisano, V.; Dam, B.; Griessen, R. *Phys. Rev. Lett.* **2009**, *102*, 226102.
(35) Parratt, L. G. *Phys. Rev.* **1954**, *95*, 359.
(36) Software available from: http://parratt32.software.informer.com/.
(37) Poulopoulos, P.; Baskoutas, S.; Papas, S. D.; Garoufalis, C. S.; Droulias, S. A.; Zamani, A.; Kapaklis, F. *J. Phys. Chem. C* **2011**, *115*, 14839; Software available from http://genx.sourceforge.net.
(38) Rehm, C.; Fritzsche, H.; Maletta, H.; Klose, F. *Phys. Rev. B* **1999**, *59*, 3142.
(39) Wojdyr, M. *J. Appl. Crystallogr.* **2010**, *43*, 1126.
(40) Birkholz, M. *Thin film analysis by X-Ray scattering*; Wiley-VCH: Weinheim, 2006.
(41) Dura, J. A.; Kelly, S. T.; Kienzle, P. A.; Her, J. H.; Udovic, T. J.; Majkrzak, C. F.; Chung, C. J.; Clemens, B. M. *J. Appl. Phys.* **2011**, *109*, 093501.
(42) Tien, H.-Y.; Tanniru, M.; Wu, C.-Y.; Ebrahimi, F. *Scripta Mater.* **2010**, *62*, 274.
(43) Fritzsche, H.; Kalisvaart, W. P.; Zahiri, B.; Flacau, R.; Mitlin, D. *Int. J. Hydrogen Energy* **2012**, *37*, 3540.
(44) Borgschulte, A.; Bösenberg, U.; Barkhordarian, G.; Dornheim, M.; Bormann, R. *Catal. Today* **2007**, *120*, 262.
(45) Schimmel, H. G.; Huot, J.; Chapon, L. C.; Tichelaar, F. D.; Mulder, F. M. *J. Am. Chem. Soc.* **2005**, *127*, 14348.
(46) Hoogeveen, R.; Moske, M.; Geisler, H.; Samwer, K. *Thin Solid Films* **1996**, *275*, 203.
(47) Higuchi, K.; Yamamoto, K.; Kajiioka, H.; Toiyama, K.; Hona, M.; Orimo, S.; Fujii, H. *J. Alloys Compd.* **2002**, *330−332*, 526.
(48) Uchida, H. T.; Kirchheim, R.; Pundt, A. *Scripta Mater.* **2011**, *64*, 935.
(49) Özgit, Ç.; Akyildiz, H.; Öztürk, T. *Thin Solid Films* **2010**, *518*, 4762.
(50) Samulevičienė, M.; Miečinskas, P.; Leinartas, K.; Grigucevičienė, A.; Kalinauskas, P.; Jasulaitienė, V.; Juškėnas, R.; Juzeliūnas, E. *Mater. Chem. Phys.* **2011**, *126*, 898.
(51) Schimmel, H. G.; Kearley, G. J.; Huot, J.; Mulder, F. M. *J. Alloys Compd.* **2005**, *404−406*, 235.
(52) Tao, S. X.; Notten, P. H. L.; van Santen, R. A.; Jansen, A. P. J. *Phys. Rev. B* **2009**, *79*, 144121.
(53) Song, Y.; Guo, Z. X.; Yang, R. *Phys. Rev. B* **2004**, *69*, 094205.
(54) Vermeulen, P.; Wondergem, H. J.; Graat, P. J. C.; Borsa, D. M.; Schreuders, H.; Dam, B.; Griessen, R.; Notten, P. H. L. *J. Mater. Chem.* **2008**, *18*, 3680.
(55) Nicolas, M.; Dumoulin, L.; Burger, J. P. *J. Appl. Phys.* **1986**, *60*, 3125.
(56) Schober, T *Solid State Phenomena*; Trans Tech Publications: Switzerland, 1996; Vol. *49−50*, pp 357−422.
(57) Friedlmeier, G.; Arakawa, M.; Hirai, T.; Akiba, E. *J. Alloys Compd.* **1999**, *292*, 107.
(58) Tan, X.; Danaie, M.; Kalisvaart, W. P.; Mitlin, D. *Int. J. Hydrogen Energy* **2011**, *36*, 2154.
(59) Ferguson, P. P.; Martine, M. L.; Dunlap, R. A.; Dahn, J. R. *Electrochim. Acta* **2009**, *54*, 4534.